A&A manuscript no.
(will be inserted by hand later)

Your thesaurus codes are:
08 (13.25.5; 10.15.2; 08.16.5; 08.03.5)

ASTRONOMY
AND
ASTROPHYSICS
25.10.1995

ROSAT X-ray observations of the young cluster IC348

Th. Preibisch[1], **H. Zinnecker**[1] & **G.H. Herbig**[2]

[1] Astronomisches Institut der Universität Würzburg, Am Hubland, D–97074 Würzburg,
Federal Republic of Germany, Internet: preib@astro.uni-wuerzburg.de; hans@astro.uni-wuerzburg.de
[2] Institute for Astronomy, 2680 Woodlawn Dr., University of Hawaii, Honolulu, HI 96822, USA

Received date ; accepted date

Abstract. We have observed the young stellar cluster IC348 in X-rays for the first time. In very deep pointings with the ROSAT PSPC and HRI we have detected a total of 116 X-ray sources. Most sources appear to be embedded ($A_V \approx 5$) in their parent molecular cloud. We use near-infrared (J, H, K) photometric data from the study of Lada & Lada (1995) to derive individual extinctions in order to calculate the X-ray luminosities. We find 56 stars to be probable new cluster members, presumably weak line T Tauri stars, because of their X-ray properties. Since previously 49 Hα emission line stars and 17 proper motion members were known, this nearly doubles the number of known member stars in IC348.

The early type (B5 – F5) stars do not appear to be intrinsic X-ray emitters. The late type stars display similar X-ray properties as those in other star forming regions. The weak line T Tauri stars seem to be stronger X-ray emitters than the classical T Tauri stars, but this difference may be caused by a selection effect. The total integrated X-ray luminosity in IC348 is at least 1.6×10^{32} erg/sec in the ROSAT band (0.1 – 2.4 keV). The possible influence of the X-radiation on the ionization state of the cloud and on its further evolution is briefly discussed.

We report the detection of several large X-ray flares in IC348 on timescales of typically a few hours. For some sources we also find variability on time scales of several years by comparing their count rates in the two pointed ROSAT observations and the ROSAT All Sky Survey. About 45% of the X-ray sources show considerable variability on long or short time scales.

Key words: X-rays: stars, open clusters: individual: IC348, pre-main-sequence stars, stellar coronae

Send offprint requests to: Th. Preibisch

1. Introduction

IC348 is a very young stellar cluster in the Perseus molecular cloud complex (Blaauw 1952) at a distance of about 300 pc (see Cernicharo et al. 1985). Its age was estimated to be $\lesssim 10^7$ yrs by Strom et al. (1974). It contains many faint ($V \approx 15 - 20$) young emission line objects, 16 of which were found in a first search for emission line stars by Herbig (1954). Up to now, 49 Hα emission stars with $W(\mathrm{H}\alpha) > 3$ Å are known in this region as a result of a new and deeper search to about $R = 19$ at the University of Hawaii 2.23 m telescope on Mauna Kea by one of us (G.H.H.). The brightest star in this region is o Per (a B1 III star with $V = 3.8$), which is thought to lie a few parsecs beyond IC348 (Bachiller et al. 1987, Snow et al. 1994) and is probably older than the cluster.

In X-rays, IC 348 is a particular challenge since most of its stars are still embedded and obscured in their protocluster parent cloud. This is because the most massive star in the cluster BD +31° 643 is only a B5 V star (see Harris et al. 1954), which is not powerful enough to disperse the cloud in which the stars were born (unlike an O star which disperses obscuring material more quickly). In their study of the density structure of the dark cloud Cernicharo et al. (1985) find visual optical extinctions exceeding 7.5 mag, while Strom et al. (1974) had estimated the mean extinction of the T Tauri stars to be about 3 – 4 mag.

Proper motion studies have been performed by Frederick (1956). Due to the rather small number of stars involved in this study, only 17 stars are known as probable cluster members. Photometric and spectroscopic observations of the brightest cluster stars have been performed by Gingrich (1922), Harris et al. (1954), and Strom et al. (1974). Due to the limiting magnitude of $V \approx 13$ in these studies, only stars with spectral type earlier than late F have been observed. We are currently performing much deeper optical observations, but this observing program is not finished yet and the results will be published in forthcoming papers.

Recently, Lada & Lada (1995) conducted a deep near-infrared (NIR) imaging survey of IC348 in the J (1.2 μm), H (1.6 μm), and K (2.2 μm) bands. The spatial resolution was $\approx 2.5''$, the limiting magnitudes were $J \approx 17$, $H \approx 16$, and $K \approx 15$. This sensitivity is good enough that nearly all cluster stars should have been found. For example, a M5 dwarf could suffer extinction up to $A_V \approx 9$ and still be above the detection threshold. In their field of $20' \times 20'$ they detected over 500 NIR sources and from comparison with several control fields they infer about 380 NIR sources to be probable cluster members. They derive a central star density of 370 stars pc^{-3}, comparable to other dense embedded young clusters like NGC 2024 in Orion. From the near-infrared color-color diagram they find that the cluster stars are typically extincted by 0.5 mag in the K band (corresponding to 4.5 mag in V) but the individual extinctions can reach considerably higher values. From their modeling of the NIR luminosity function of IC348 they conclude that continuous star formation has taken place in the last $\approx 6 \times 10^6$ years. E. Lada kindly provided us with the table of the positions and magnitudes of the sources.

In the dark cloud a few arcminutes south-west of IC348 Strom et al. (1974) detected a small red reflection nebula and a bright infrared source, IC348-IR. From the near-infrared colour indices they assumed this to be a deeply embedded ($A_V \approx 20 - 30$) B star. In order to search for more embedded objects, McCaughrean et al. (1994) recently made a near-infrared survey of the surroundings of IC348-IR. They could not find other embedded sources, but they discovered a very young (< 1000 yrs) molecular hydrogen jet (HH211).

2. X-ray observations and data analysis

2.1. The PSPC observation

On August 25 and 26 1992 IC348 was observed for 23 675 sec with the ROSAT position sensitive proportional counter (PSPC). This instrument has an effective area larger than the EINSTEIN IPC or the EXOSAT LE, very low particle background, and an excellent pulse-height discrimination. It has a moderate energy resolution of $\Delta E/E \approx 0.4$ at 1 keV and a spatial resolution (FWHM) of about $25''$. The total field of view is circular with a radius of $1°$. A detailed description of this instrument can be found in Trümper et al. (1991).

The observation was split into 13 time intervals lasting between 800 and 2000 sec. The analysis of the ROSAT observation data was performed with the EXSAS software package (Zimmermann et al. 1993). The central part of the PSPC image is shown in Fig. 1.

In our analysis of the data we determined the positions of the X-ray sources, the background corrected source count rates, and the hardness ratios. Spectral modeling was carried out for sources with a sufficient number of X-ray counts. We also investigated the X-ray lightcurves of the sources to search for variability.

During our observation a giant X-ray flare occurred on the classical T Tauri star LHα 92. A detailed analysis of this event has been presented in Preibisch et al. (1993).

As can be seen in Fig. 1, there is a dense cluster of X-ray sources at the center of IC348. Closer inspection of the data showed that this cluster could not be resolved with the spatial resolution of the PSPC. This was the reason for us to ask for additional observing time with the ROSAT High Resolution Imager.

2.2. The HRI observation

From August 15 1994 to August 26 1994 IC348 was observed for 44 386 sec with the ROSAT High Resolution Imager (HRI). This is a micro-channel plate detector with an excellent spatial resolution (FWHM $\approx 5''$), but no energy resolution. The field of view is about $40' \times 40'$ and the sensitivity of the HRI is a factor of about 2.5 less than that of the PSPC (see section 5). A detailed description of this instrument can be found in Trümper et al. (1991) or David et al. (1993). The central part of the HRI image is shown in Fig. 2.

2.3. Source detection and Identification

The source detection was done separately in the PSPC and the HRI images by a four step procedure. In the first step a "sliding-window" technique was applied, where the counts found in a window and in a background region around this window are compared to find possible sources. In the second step these sources were cut out of the image. Applying a spline fit to this cheesed image, a smoothed background image was constructed. Now again, another sliding window technique was applied, where the counts in the window were compared to the counts in the same window position in the background image. Both steps were performed on the image including all photon energies and on images containing only the soft (0.1 – 0.4 keV) resp. hard (0.4 – 2.4 keV) photons. The lists of possible sources were merged and in the third step each possible sources was investigated in detail with a maximum likelihood method, in which the probability that the observed distribution of counts is due to a statistical background fluctuation was determined. All possible sources for which this probability is less than e^{-10} (corresponding to a 4.8σ detection) were accepted as real sources. For the accepted sources the observed distribution of counts was fitted to a source model to find the most likely values for the background and source strength, the position of the source, and the errors of these parameters.

All three steps described so far are carried out by an automatic process in EXSAS. Such automatic detection methods are sometimes known to have difficulties (especially in crowded regions, where the mean distance of the

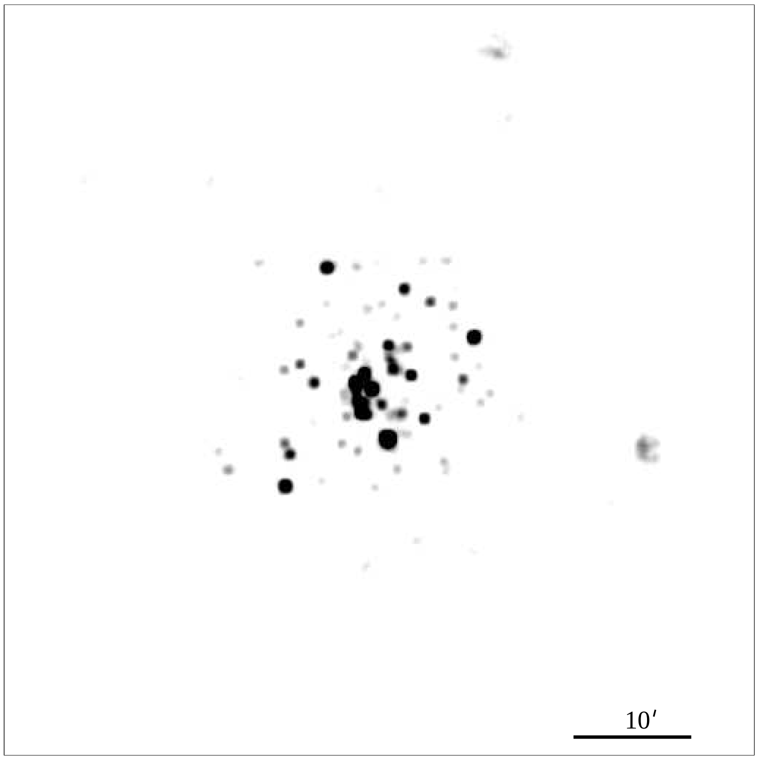

Fig. 1. Central part of the PSPC image of IC348. The field shown is $64' \times 64'$. To create this image we binned the photon events file in $7.5'' \times 7.5''$ pixels and smoothed it with a gaussian function.

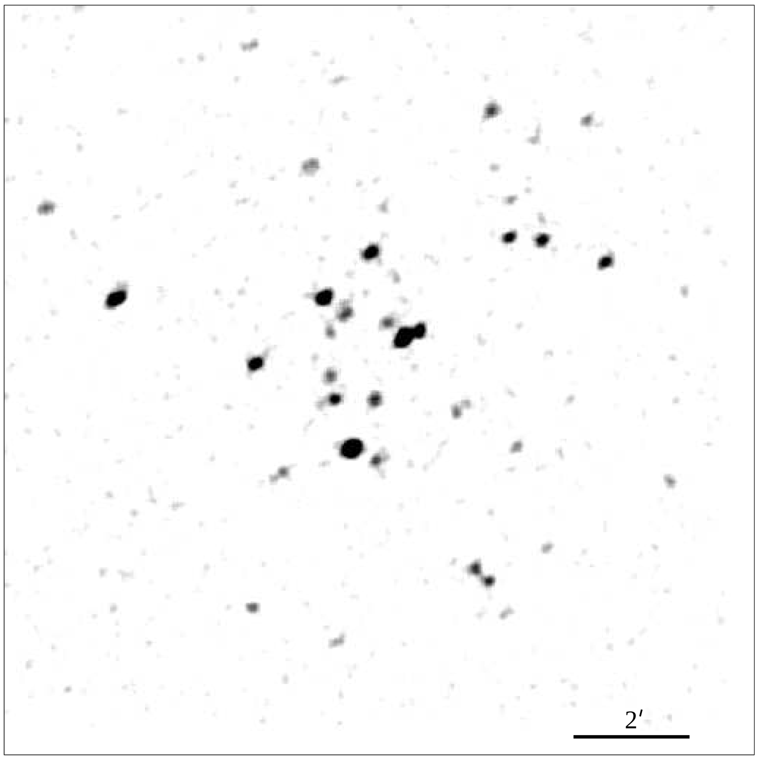

Fig. 2. Central part of the HRI image of IC348. The field shown is $13' \times 13'$. To create this image we binned the photon events file in $1.5'' \times 1.5''$ pixels and smoothed it with a gaussian function.

sources is less or comparable with the width of the point-spread-function). As one can see from Fig. 1, the density of sources is very high in the central cluster. The automatic detection method interpreted this cluster as a single "extended" source in the PSPC image. So the fourth step was to check these results by eye. We also included sources of the central cluster with a signal to noise ratio $S/N >$ 3 in the list of sources. With the exception of the dense central cluster the results of the SASS source list, the EXSAS source detection procedure and the visual impression showed good agreement.

In the HRI image no source confusion occurred due to the much better spatial resolution. In total, we found 108 X-ray sources in the PSPC image and 55 sources in the HRI image.

By trying to identify the PSPC sources, we noted a systematic error of $12''$ in declination. After correcting for this shift optical counterparts could be found for nearly all PSPC sources and the positions matched the corresponding HRI source positions very well. This shift is probably due to a boresight error in the ROSAT aspect system. Then we merged the two source lists into a single X-ray source list. This final source list contains 116 sources. To check the accuracy of the positions, we used the *Hubble Space Teleskope Guide Star Catalog* (GSC; Lasker et al. 1990) and could find optical counterparts for 28 X-ray sources. We did not find any systematic deviation of the X-ray source positions from the optical positions; the mean discrepancies are about $2''$ in declination as well as in right ascension.

A close inspection of the HRI data showed a slight elongation of the source images. This is probably caused by problems with the long term stability of the satellite attitude control in such a long (> 12 hours) pointing (C. Izzo, priv. comm.). This elongation does not cause any problems in the determination of the count rates, if appropriate source extraction radii are used.

For further identification of the X-ray sources we used the SIMBAD database, the Herbig-Bell Catalog and the IRAS catalogs. We also used the star positions of Frederick (1956) and Strom et al. (1974), the optical images of Gingrich (1922), and Herbig (1954), and the Palomar Observatory Sky Survey (POSS) plate. For the central region of IC348 we used direct images obtained at the UH 2.23 m telescope on Mauna Kea (see Section 4.2.1) and images taken for us by I. Thiering at the 1.23 m telescope on Calar Alto. A source was assumed to be identified, if the positional deviation was less than the 3σ error of the X-ray position, but most identifications had much smaller deviations. In some cases several possible optical counterparts were located in the X-ray position error circle. In these cases we preferred the closest positional match. In Table 1 we give the positions of the X-ray sources denoted as IC348-X (or simply X- in the text) together with the positional uncertainties derived with the maximum likelihood method. For the identification we use the LkHα or IfAHα number for the Hα stars (see paragraph 4.2.1). G denotes the star numbers given in Gingrich (1922), F those in Frederick (1956). For unnamed stars we use the GSC number. The letter O means that an optical counterpart for the X-ray source could be found on the Palomar Sky Survey plate or in our optical images. Sources for which we could not find an optical counterpart but which could be identified with a NIR source from the study of Lada & Lada (1995) are marked with "NIR". For the objects where we have accurate optical positions we also give the deviation between optical and X-ray position in the last column of Table 1.

For 16 sources (14%) we could not find an optical counterpart. Six of them are located inside the field of the NIR study and for all six we could find NIR counterparts. This indicates that the other 10 unidentified sources are probably obscured too heavily to be optical visible. This possibility is affirmed by the fact that 6 of these 10 sources lie in the direction of the dark clouds around IC348 (they are marked with (D) in Table 1).

For all X-ray sources located in the region investigated by Lada & Lada (1995) we could find NIR counterparts. There are 75 IRAS Point Source Catalog sources in the field of view, but only four of them are coincident with X-ray sources: X-36 (= o Per) can be identified with the IRAS source 3411+3207, X-89 with IRAS 3417+3207, X-2 with IRAS 3385+3149 and X-15 with IRAS 3406+3144. No X-ray source could be detected at the postition of the strongest IRAS source in the field of view, IRAS 3414+3200, located $\approx 30''$ south-east of BD $+31°643$. Neither IC348-IR nor the jet HH 211 could be detected in X-rays.

2.4. Determination of count rates and upper limits

In order to determine count rates a detailed investigation of the instrumental point spread function (PSF) is necessary. The PSF of the PSPC is a rather complicated function of the photon energy and the off-axis angle of the source. We simulated several theoretical PSFs for sources with Raymond & Smith plasma spectra for temperatures of log $T = 6$ and log $T = 7$ and hydrogen column densities between $10^{19}\,\mathrm{cm}^{-2}$ and $10^{22}\,\mathrm{cm}^{-2}$. The encircled source flux at a given radius of the source region was then calculated by numerical integration. We found that for source regions larger than $50''$ the encircled fraction of the source flux can be very well approximated by that of the monochromatic PSF for 1 keV photons. We decided to use a source region radius that contains at least 95% of the 1 keV source counts. At the center of the PSPC field this corresponds to a radius of $\approx 80''$. For several sources especially in the central regions these source circles would overlap and we had to reduce the radius until the overlap was removed. To take into account the loss of counts due to this reduction, we calculated the encircled fraction of source counts from

Table 1. Positions, count rates and identifications of the X-ray sources (for details see text).

IC348-X	RA	DEC	±	PSPC count rate		HRI count rate		Identification	Δ
	(J2000)	(J2000)	[″]	[cnts/ksec]	±	[cnts/ksec]	±		[″]
1	3 41 04.9	32 12 32	15	10.7	5.7			O	
2	3 41 34.8	31 57 41	15	9.6	5.0			IRAS 3385+314	
3	3 42 17.2	31 41 08	9	7.9	5.2			–	
4	3 42 42.7	32 03 41	10	10.8	1.9			O	
5	3 43 07.7	32 10 28	9	3.3	1.2			O	
6	3 43 33.2	32 06 23	6	2.5	1.0	<0.6		O	
7	3 43 36.3	32 31 51	16	5.3	1.7			O	
8	3 43 42.8	32 37 48	16	18.1	2.5			HD 281153	28
9	3 43 44.5	32 08 17	2	2.2	0.5	2.2	0.5	LHα86	1
10	3 43 48.6	32 15 51	9	2.1	0.6	<0.3		O	
11	3 43 48.8	32 07 31	3	2.2	0.5	1.3	0.4	O	
12	3 43 49.3	32 18 05	8	1.2	0.6	1.1	0.5	O	
13	3 43 49.5	32 10 40	5	2.0	0.4	<1.0		O	
14	3 43 51.2	32 13 09	2	23.3	1.3	6.5	0.7	G2	<1
15	3 43 53.0	31 55 00	10	3.2	1.2	<0.3		(D)	
16	3 43 55.4	32 09 32	2	5.5	0.6	0.8	0.4	GSC 2359 848	<1
17	3 43 55.8	32 08 39	5	1.7	0.4	<0.3		O	
18	3 43 58.8	32 11 23	4	2.5	0.5	0.7	0.2	LHα88	4
19	3 43 58.9	32 17 31	7	1.4	0.4	<0.5		LHα87	7
20	3 43 59.6	32 14 03	2	1.7	0.5	3.5	0.5	NIR	
21	3 44 00.3	32 15 58	4	2.7	0.5	<0.6		O	
22	3 44 02.2	32 19 37	5	3.4	0.6	<1.1		NIR	
23	3 44 02.6	32 01 34	7	1.9	0.5	<0.4		O	
24	3 44 03.9	32 02 40	6	2.6	0.5	<0.7		O	
25	3 44 04.7	32 25 03	15	0.8	0.6	<0.5		O	
26	3 44 05.2	32 07 11	5	1.7	0.4			O	
27	3 44 05.3	32 10 00	8	0.8	0.3	<0.4		GSC 2359 894	9
28	3 44 08.8	32 16 12	3	5.2	0.8	1.7	0.5	GSC 2359 286	2
29	3 44 10.1	32 09 24	3	<0.4		0.7	0.2	NIR	
30	3 44 11.3	32 06 09	2	4.4	0.8	0.8	0.3	O	
31	3 44 11.6	32 19 40	5	3.0	0.6	<0.6		O	
32	3 44 14.2	31 55 47	6	3.0	1.0	<0.5		(D)	
33	3 44 15.0	31 16 31	9	43.1	4.4			O	
34	3 44 16.5	32 09 54	2	9.9	0.8	1.8	0.3	GSC 2359 821	3
35	3 44 18.0	32 12 19	2	4.4	0.6	1.0	0.2	O	
36	3 44 19.2	32 17 19	1	8.3	1.0	11.0	0.7	oPer	3
37	3 44 20.2	31 59 36	9	0.5	0.4	<0.3		(D)	
38	3 44 20.2	32 06 37	9	4.8	0.6			O	
39	3 44 21.3	32 05 01	3	<0.9		0.8	0.2	IfAHα16	1
40	3 44 21.4	32 15 09	3	1.8	0.4	0.1	0.3	O	
41	3 44 21.6	32 10 16	2	3.1	0.5	1.7	0.2	LHα90	1
42	3 44 21.6	32 10 38	3	1.7	0.6	0.5	0.2	IfAHα21	1
43	3 44 22.2	32 01 54	4	3.6	0.9	<0.2		O	
44	3 44 22.2	32 12 00	3	1.9	0.4	0.7	0.2	LHα91	1
45	3 44 23.7	32 06 45	3	1.9	0.4	0.7	0.2	IfAHα58	2
46	3 44 24.1	32 10 58	2	4.5	0.5	0.6	0.2	G8	3
47	3 44 24.2	32 10 19	2	5.5	0.6	1.6	0.2	O	6
48	3 44 24.7	32 03 52	3	<1.5		0.4	0.2	NIR	
49	3 44 25.7	32 12 29	2	9.1	0.8	1.5	0.3	GSC 2359 632	2
50	3 44 25.7	32 11 26	9	3.6	0.5	<0.3		IfAHα24	5
51	3 44 25.9	32 04 27	2	2.8	0.4	1.1	0.2	LHα92	3
52	3 44 27.0	32 04 40	2	7.3	1.2	1.2	0.2	O	
53	3 44 28.1	32 16 03	3	2.1	0.4	0.4	0.3	O	
54	3 44 28.5	32 07 22	3	6.4	0.6	0.9	0.2	GSC 2359 815	1
55	3 44 29.5	32 25 47	10	1.0	0.6			GSC 2359 943	12
56	3 44 30.3	32 19 23	6	2.0	0.8	<0.6		O	
57	3 44 31.4	32 08 44	2			2.1	0.3	O	
58	3 44 31.6	32 00 19	5	2.1	0.7	<0.2		NIR	

Table 1. – Continued

IC348-X	RA (J2000)	DEC (J2000)	± [″]	PSPC count rate [cnts/ksec]	±	HRI count rate [cnts/ksec]	±	Identification	Δ [″]
59	3 44 32.8	32 08 36	1	26.3	1.2	5.6	0.4	O	6
60	3 44 33.3	32 09 37	3	< 2.1		0.2	0.2	NIR	
61	3 44 34.0	32 08 52	3			1.1	0.2	O	
62	3 44 34.1	32 10 50	9	1.0	0.4	< 0.6		IfAHα55	1
63	3 44 34.9	32 06 31	2	7.8	1.9	1.1	0.2	GSC 2359 809	3
64	3 44 35.1	32 07 33	2	6.4	0.6	1.4	0.2	LHα94	4
65	3 44 35.4	32 10 04	2	17.5	1.0	2.0	0.3	G12	
66	3 44 35.4	32 15 38	6	2.7	0.5			O	
67	3 44 35.4	31 53 31	8	2.2	1.0	< 0.7		(D)	
68	3 44 36.9	32 06 44	1	22.6	1.2	6.8	0.4	G13	2
69	3 44 37.5	32 09 02	2	4.5	0.6	1.2	0.2	IfAHα57	2
70	3 44 37.7	32 12 21	9	2.1	0.4	< 0.3		O	
71	3 44 38.0	32 03 26	3	2.2	0.5	0.8	0.2	GSC 2359 829	4
72	3 44 38.3	32 07 34	2	9.2	0.7	1.5	0.2	O	2
73	3 44 38.6	32 08 41	2	7.3	1.5	0.7	0.2	O	1
74	3 44 38.6	32 07 58	2	4.3	0.7	1.0	0.2	IfAHα36	3
75	3 44 39.2	32 09 18	2	17.6	1.0	3.2	0.3	O	1
76	3 44 39.4	32 19 05	5	3.1	0.6	< 0.4		O	
77	3 44 40.3	32 11 32	2	3.3	0.5	1.3	0.2	GSC 2359 1002	3
78	3 44 41.8	32 23 17	8	0.7	0.4	< 0.6		O	
79	3 44 42.0	32 08 59	9	0.9	0.4	< 0.2		IfAHα40	1
80	3 44 42.4	32 06 19	2	2.6	0.4	0.8	0.2	O	
81	3 44 42.6	32 17 59	9	0.9	0.3	< 0.3		O	
82	3 44 43.0	32 07 41	9	1.1	0.3	< 0.2		O	
83	3 44 43.5	32 08 32	9	1.0	0.5	< 0.2		IfAHα45 (?)	11
84	3 44 43.8	32 08 12	9	1.2	0.5	< 0.1		GSC 2359 759	7
85	3 44 44.7	32 08 10	2	< 1.3		1.0	0.1	IfAHα46	3
86	3 44 44.9	32 04 00	2	1.9	0.5	1.4	0.5	LHα97	4
87	3 44 45.1	32 13 36	3	0.9	0.7	0.6	0.2	O	
88	3 44 50.8	32 19 07	2	18.3	1.1	6.8	0.7	G16	2
89	3 44 50.9	32 16 09	4	1.4	0.4	0.7	0.4	O	
90	3 44 52.0	31 58 50	10	0.9	0.6	< 0.4		(D)	
91	3 44 52.0	32 00 49	5	1.3	0.4			O	
92	3 44 53.7	32 06 56	8	0.9	0.4	< 0.2		O	
93	3 44 55.8	32 05 43	6	1.2	0.4	< 0.2		O	
94	3 44 55.9	32 09 16	2	5.9	0.8	3.8	0.3	LHα98	2
95	3 44 58.4	32 59 23	16	39.4	5.2			–	
96	3 45 00.1	32 17 38	10	0.5	0.3	< 0.5		–	
97	3 45 01.5	32 14 21	4	2.3	0.8	< 0.6		O	
98	3 45 01.6	32 10 49	2	4.6	0.6	1.5	0.3	GSC 2360 372	3
99	3 45 02.7	32 06 58	7	0.4	0.3	< 0.3		O	
100	3 45 03.7	32 09 31	16	0.5	0.3	< 0.1		O	
101	3 45 05.9	32 03 03	3	7.7	0.7	0.9	0.3	O	
102	3 45 07.7	32 10 28	3	3.3	0.5	0.7	0.3	G17	3
103	3 45 07.9	32 00 24	2	19.5	1.3	8.5	0.7	G18	4
104	3 45 08.2	32 04 00	4	4.4	0.5	0.2	0.3	GSC 2360 54	4
105	3 45 14.5	32 25 59	12	1.6	0.7			O	
106	3 45 18.4	32 12 12	8	0.5	0.4	< 0.6		O	
107	3 45 18.6	32 19 36	5	2.4	0.9	< 0.5		O	
108	3 45 22.0	32 02 06	9	0.8	0.4	< 0.7		O	
109	3 45 24.0	32 24 45	11	1.4	0.7			O	
110	3 45 25.9	32 09 37	8	0.7	0.4	< 0.8		GSC 2360 562	19
111	3 45 30.7	32 01 55	5	4.9	0.7	0.5	0.9	GSC 2360 67	1
112	3 45 33.5	31 56 42	8	1.1	0.9	8.8	1.3	O	
113	3 45 34.3	32 03 25	6	2.7	0.5	< 1.0		O	
114	3 45 38.2	32 26 45	16	10.4	1.7			F23	15
115	3 46 28.7	32 26 55	15	14.0	2.1			–	
116	3 47 25.3	32 28 48	17	12.5	3.6			(D)	

the theoretical PSF for 1 keV and corrected the number of source counts for this effect.

The PSF of the HRI is nearly independent of the photon energy. From the off-axis angle one can easily calculate the extraction radius containing a certain fraction of the source counts. We took into account the elongation of the source images by using a large enough extraction radius that certainly includes more than 99% of the source counts.

To calculate background subtracted count rates we took the background counts out of an annulus concentric with but outside of the source circle. For a few HRI sources in regions with very high source density and for most of the PSPC sources this was not possible because there would have been an overlap between the background regions and the source region of other sources. In these cases the background regions were chosen in source free regions as close as possible to the source region. The count rates are given in Table 1. Note that for the sources showing a flare during the observation we give the count rates in the pre-flare state. In the area common to the PSPC and the HRI observations we determined upper limits of the HRI count rates of PSPC sources not detected in the HRI image and vice versa. This was done by comparing the counts in a detection cell at the target position with that of several nearby background regions. The 90% confidence upper limits calculated according to Kraft et al. (1991) are given in Table 1.

There are two cases in which the HRI observation could resolve a single PSPC source into multiple sources. The first case refers to the sources X-51 and X-52. They have a distance of 18″ and both have visual and near-infrared counterparts. The PSPC PSF has a FWHM of 24″ for 1 keV photons at this position, so in principle the sources should just be resolved in the PSPC image. This is not the case, because of the giant flare that occurred on LHα 92 = X-51 during the PSPC observation. Due to this, only the flare source X-51 was found and X-52 escaped detection. To resolve the sources in the PSPC data, we selected only photons that arrived before the flare. Since we knew the source positions from the HRI observation, we could model the strongly overlapping PSFs and determine the count rates. The results of the analysis of the flare on LHα 92 based only on the PSPC observation in Preibisch et al. (1993) are hardly influenced. The count rate rise factor is more than 300 and due to this giant amplitude the few counts coming from X-52 do not influence the X-ray properties during the flare.

The second case refers to the sources X-57, X-59, and X-61. All three sources are within 33″ and thus cannot be resolved in the PSPC image. All three HRI sources have optical and near-infrared counterparts, but there are two additional near-infrared sources: One very close to X-59 and one between X-57 and X-60. Since it cannot be excluded that one of these stars contributes to the X-ray emission, we did not try to deconvolve the PSPC counts.

3. Calculation of X-ray luminosities

We interpreted the X-ray spectra as optically thin plasma emission (see Raymond & Smith 1977). Interstellar absorption leads to strongly energy dependent extinction effects, especially at low energies (see Morrison & McCammon 1983). Therefore the knowledge of extinction is very important for the calculation of X-ray luminosities.

In IC348 the visual extinction exceeds 7.5 mag in some directions (Cernicharo et al. 1985). Using the relation $N_{\rm H} = A_V \times 1.8 \times 10^{21}\,{\rm cm}^{-2}$ (Paresce 1984; Predehl & Schmitt 1995) this extinction corresponds to a hydrogen column density of $N_{\rm H} \approx 1.3 \times 10^{22}\,{\rm cm}^{-2}$. The minimum extinction for a star at the front of the cluster can be estimated by multiplying the average hydrogen density $n_{\rm H} = 0.07\,{\rm cm}^{-3}$ (Paresce 1984) with the distance of 300 pc. This gives $N_{\rm H} \approx 6.5 \times 10^{19}\,{\rm cm}^{-2}$ along the line of sight towards the front side of the cluster. Thus $N_{\rm H}$ towards the cluster stars can vary by a factor of 200 or even larger, since we did not consider circumstellar extinction, which may be significant for T Tauri stars. Thus, a reasonable determination of X-ray luminosities is possible only if individual extinctions of the sources are known. In principle, the extinction can be determined from the fit to the X-ray spectrum, but this is possible only for the strongest sources with high quality spectra. For the majority of the weaker sources we must determine the extinction from optical or NIR measurements.

3.1. Extinction towards the X-ray sources

There are only two stars for which detailed extinction information is available: For o Per Snow et al. (1994) found $N_{\rm H} = 1.6 \times 10^{21}\,{\rm cm}^{-2}$ and for BD +31° 643 they found $N_{\rm H} = 3.7 \times 10^{21}\,{\rm cm}^{-2}$. For 17 stars from the list of Gingrich (1922) Strom et al. (1974) have determined the optical extinctions from their V and K magnitudes.

For most of the X-ray sources the only way to get some information about extinction is to estimate it from the NIR colours. This puts up two problems: First, for embedded sources the derived extinction depends on the distribution of the circumstellar matter. For example, a disk seen pole on causes an IR excess but does not contribute very much to the extinction. To minimize the possible error we use the J and H magnitudes, since the contribution of a disk is small at these short wavelengths and increases to longer wavelengths. Second, since we have no spectral classification, we do not know the intrinsic colours of the stars and have to assume a reasonable value. To do this, we first split the stars into two groups according to their position in the NIR colour-colour diagram (see Fig. 5). All stars with colours consistent to those of reddened main-sequence stars are assumed to have no NIR excess. All stars lying below the reddening line for M6 dwarfs are classified as NIR excess stars. For stars showing no NIR excess, we use $(J-H)_0 = 0.6$, which is correct for a K5 dwarf. In the spectral range from K2 to M6 the deviation from the correct $(J-H)_0$ colour is less than 0.1, for a G0 star it is 0.3 (Bessell & Brett 1985). In principle, the intrinsic NIR colours of pre main-sequence stars may be different from those of main-sequence stars. Recently, Kunkel (1995) has determined the intrinsic colours of the T Tauri stars in the Scorpius-Centaurus region and found that the NIR colours are very similar to those of main-sequence stars. For spectral types between K0 and M6 he found $(J-H)_0$ to vary between 0.5 and 0.65. This justifies our assumption of $(J-H)_0 = 0.6$ for stars without NIR excess.

For stars with evidence for a NIR excess we use $(J-H)_0 = 0.8$ since this was found by Strom et al. (1994) to be the typical $(J-H)_0$ for classical T Tauri stars.

To calculate the extinction from $E(J-H)$, we used the relations $A_J = 2.64 \times E(J-H)$ (Greene et al. 1994) and $A_{V,IR} = 3.55 \times A_J$ (Rieke & Lebofsky 1985). From the maximum error in $(J-H)_0$ of $+0.1$ and -0.3 for no-excess stars we can estimate the maximum error in A_V to be $+0.94$ and -2.81. For NIR excess sources this error in $(J-H)_0$ is $\approx \pm 0.3$. The resulting errors in $\log L_{\mathrm{X}}$ are about ± 0.3.

3.2. Spectral fitting

The simplest spectral model for coronal sources is to assume isothermal plasma emission, which leads to a model with 3 parameters: The plasma temperature T, the emission measure EM, and the hydrogen column density N_{H}. For fitting the observed count rate spectra, one calculates the photon flux according to the theoretical model. This flux is folded with the response function of the telescope to give the theoretical count rate spectrum and this spectrum is compared to the observed count rate spectrum. The theoretical model is then adjusted to minimize the deviations between the observed and the theoretical count rate spectra. It must be emphasized that there are several difficulties in such a procedure:

First, the results of spectral fitting only make sense if the assumed model is correct. While the adopted model leads to a satisfactory statistical description for most stellar X-ray spectra, there are indications that at least the spectra with high S/N ratio require a two temperature or even a continuous emission measure model (see Schmitt et al. 1990). However, in consideration of the rather low S/N for our spectra we did not attempt more complex than single temperature fits. The only exception is X-14, where we had extinction information and could not find an acceptable one temperature fit. A two temperature model reproduced the spectrum very well (see Fig. 3).

The second problem is the moderate spectral resolution ($\Delta E/E \approx 0.4$ at 1 keV) of the PSPC. In the temperature range of interest between $\log T = 5$ and $\log T = 7.5$ the spectra are dominated by many strong emission lines. These lines can not be resolved and the continuum emission changes only rather weakly as a function of temperature. To prove the capability of the PSPC of determining the spectral parameters, we have performed a large number of spectral fits to simulated spectra. This will be described in a forthcoming paper (Preibisch et al., in preparation, see also Maggio et al. 1995). These simulations demonstrate that the X-ray luminosities can be reproduced with typical errors $\lesssim 20\%$ even for spectra with no more than 200 counts.

The last problem is the small number of counts for most sources. This results in large errors in the spectra and accordingly large uncertainties in the fitted parameters. Based on our experience from the spectral fitting simulations, we extracted and fitted spectra only for sources with more than 150 source counts.

3.2.1. Fitting procedure and results

The PSPC has 243 calibrated pulse height channels. Given the rather low spectral resolution of the PSPC, the spectrum is highly oversampled and has to be rebinned before the fit. We binned the spectrum in such a way that the background subtracted count rate in each bin exceeded a signal to noise ratio of $S/N \geq 5$.

The best fit model was determined by a χ^2 minimizing procedure. To evaluate the quality of the fit we used χ^2_{min} to calculate the "statistical acceptance" Q, which gives the probability that the deviations between the data and the best fit model can be explained by statistical measurement errors (see Press et al. 1986). We rejected fits with $Q < 0.01$, because there is a 99% probability that the deviations are due to a wrong model and not only statistical measurement errors.

To find the global minimum of the χ^2 statistic, we started the fit algorithm from several different points in the parameter space. To derive the confidence regions for the fitting parameters we used the projection method of Lampton et al. (1976).

For 14 sources we could find an acceptable fit. In Table 2 we give the best fit parameters, the 1σ error for N_{H} and $\log T$ (independent of each other), as well as χ^2_{red}. If extinction information was available in the literature, we fixed N_{H} to this value in the fit. In these cases no errors are given for N_{H} in Table 2.

X-33 is the only source showing very low extinction (the fit is consistent with negligible extinction and gives only an upper limit to the hydrogen column density) and a plasma temperature clearly below 10^7 K. These properties and its position more than $50'$ away from the center of IC348 suggest this source to be a foreground object. All other spectra show strong extinction which causes very low count rates in the soft channels below 0.5 keV. For several sources the fit gave two acceptable models, one model with N_{H} above $10^{22}\,\mathrm{cm}^{-2}$ and low T and the other with lower N_{H} and higher T. The X-ray luminosities computed from these models are sometimes different by more

Table 2. Results of spectral fitting. If no errors are given for $N_{\rm H}$, the extinction was fixed to the given value (see text).

IC348-X	log $N_{\rm H}$ [cm^{-2}]	log T [K]	$\chi^2_{\rm red}$	log $L_{\rm X}$ [erg/sec]
14	21.5	$6.2^{+0.2}_{-0.2}+7.2^{+0.1}_{-0.1}$	0.45	$31.4^{+0.2}_{-0.2}$
33	< 20.3	$6.4^{+0.1}_{-0.2}$	1.55	
34	$21.0^{+0.3}_{-0.2}$	$7.2^{+0.1}_{-0.1}$	0.29	$30.2^{+0.2}_{-0.3}$
36	21.2	$7.0^{+0.1}_{-0.1}$	1.66	$30.1^{+0.1}_{-0.1}$
49	$21.0^{+0.5}_{-0.2}$	$7.4^{+0.6}_{-0.1}$	1.06	$30.2^{+0.3}_{-0.3}$
65	21.7	$7.1^{+0.1}_{-0.1}$	1.41	$30.9^{+0.1}_{-0.1}$
68	21.8	$7.1^{+0.1}_{-0.1}$	0.75	$31.0^{+0.1}_{-0.1}$
72	$21.8^{+0.1}_{-0.3}$	$7.1^{+0.1}_{-0.1}$	1.64	$30.7^{+0.2}_{-0.4}$
75	$21.6^{+0.2}_{-0.1}$	$7.7^{+0.5}_{-0.2}$	0.60	$30.8^{+0.2}_{-0.3}$
88	21.8	$7.2^{+0.1}_{-0.1}$	0.33	$31.0^{+0.1}_{-0.1}$
101	$20.9^{+0.2}_{-0.1}$	$7.9^{+0.3}_{-0.2}$	1.31	
103	21.3	$7.2^{+0.1}_{-0.1}$	1.25	
115	$22.2^{+0.1}_{-0.1}$	$6.7^{+0.2}_{-0.2}$	1.25	
116	$21.8^{+0.3}_{-0.8}$	$7.1^{+0.2}_{-0.5}$	0.42	

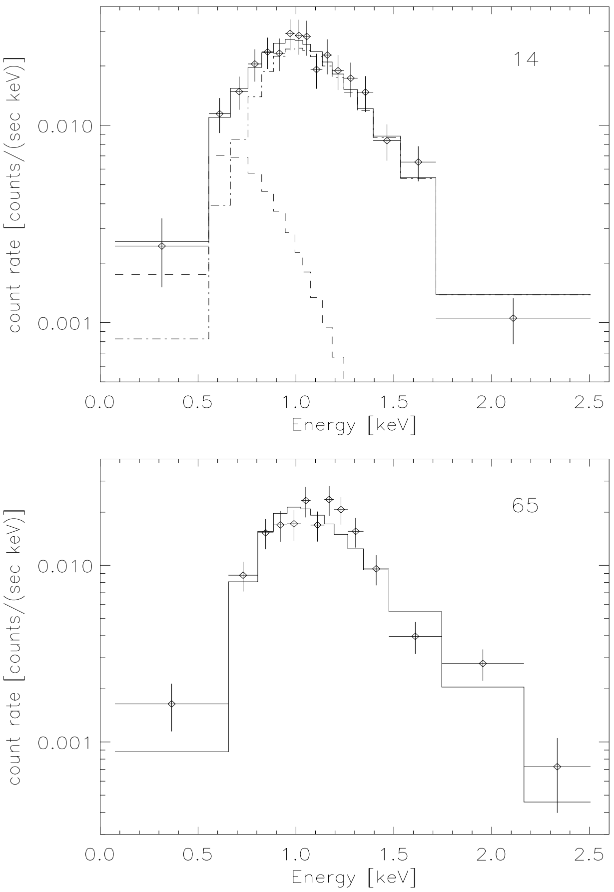

Fig. 3. X-ray spectra of the sources X-14 and X-65. The diamonds with the error bars are the background subtracted spectra, the solid lines are the fitted model spectra. For X-14 a two temperature model was used, the dashed line shows the contribution of the low temperature component, the dashed-dotted line that of the high temperature component.

than one order of magnitude. In all these cases the extinction required for the model with lower $N_{\rm H}$ was in good agreement with the estimate for $A_{V,IR}$. So we preferred the models giving the smaller $N_{\rm H}$. The plasma temperatures obtained are typical for active late type stars (see Schmitt et al. 1990). For sources more than $30'$ away from the cluster center we did not calculate X-ray luminosities because they are probably non-members and so we do not know their distances.

In Fig. 3 we show two examples of the spectral fits. The first is the spectrum of X-14 (= G2) that needed a two temperature model for a reasonable fit. The second is X-65 (= G12). Here, an effect found in several spectra can be seen: The model spectrum calculated with $N_{\rm H}$ fixed at the value computed from A_V shows too few soft X-ray counts. This indicates that a better fit to the X-ray spectrum could be achieved if a smaller $N_{\rm H}$ were used. In fact, a fit treating $N_{\rm H}$ as free parameter finds a slightly better fit ($\chi^2_{\rm red} = 1.26$ instead of 1.41) and gives $N_{\rm H} = 2.0^{+1.6}_{-0.5} \times 10^{21}\,{\rm cm}^{-2}$. The fit with $N_{\rm H}$ as free parameter gives an X-ray luminosity of log $L_{\rm X} = 30.6$, while that with $N_{\rm H}$ fixed at the "optical" value $5.7 \times 10^{21}\,{\rm cm}^{-2}$ gives log $L_{\rm X} = 30.9$. This shows that the determination of X-ray luminosities from strongly extincted spectra with low S/N has severe uncertainties. Since we cannot clarify this situation with the available spectra, we use the X-ray luminosity found with $N_{\rm H}$ fixed at the "optical" value.

3.3. X-ray luminosity for weaker sources

For the sources with too few counts for spectral fitting we computed a count rate to flux conversion factor. This was done by using the extinction estimated from the NIR colours and assuming a plasma temperature of $T = 10^7$ K. A model spectrum calculated from these parameters was folded through the response function of the telescope to obtain the model count rate. From the unreddened energy flux of the model spectrum we can then calculate the energy flux of the source from the ratio of measured count rate to model count rate. The resulting X-ray luminosities are given in Table 3.

Table 3. Near infrared magnitudes (from Lada & Lada 1995), extinctions derived from the NIR colours, and X-ray luminosities of sources that are neither known proper motion members nor Hα stars; the estimated error in log L_X is ± 0.3.

IC348-X	J [mag]	H [mag]	K [mag]	$A_{V,IR}$ [mag]	log L_X [erg/sec]	IC348-X	J [mag]	H [mag]	K [mag]	$A_{V,IR}$ [mag]	log L_X [erg/sec]
6	12.0	11.4	11.1	0.5	29.6	54	11.7	10.9	10.7	1.5	30.2
10	12.9	12.1	11.7	1.4	29.7	56	12.3	11.5	11.1	2.0	29.8
11	12.3	11.5	11.2	1.2	29.8	57	10.6	9.9	9.7	0.4	29.8
12	12.4	11.6	11.3	2.1	29.9	58	13.4	11.7	10.5	8.8	30.9
13	12.6	11.8	11.5	1.3	29.7	59	10.1	9.6	9.4	0.1	30.5
16	11.2	10.6	10.3	0.4	29.9	60	12.2	11.4	11.0	2.0	29.2
17	12.6	11.8	11.5	2.4	29.8	61	11.7	10.9	10.7	1.6	29.8
20	12.1	11.3	11.0	2.4	30.5	63	11.4	10.6	10.3	2.0	30.4
21	13.0	12.0	11.6	3.4	30.2	66	13.1	12.3	11.9	2.1	30.0
22	12.3	11.5	11.3	1.7	30.0	70	12.9	11.8	11.2	4.4	30.3
23	12.7	12.0	11.7	0.7	29.5	71	11.2	10.4	10.1	2.1	29.9
24	13.5	12.9	12.6	0.1	29.5	72	11.2	10.3	9.9	2.9	30.7
26	13.2	12.4	12.0	0.1	29.3	73	11.1	10.0	9.5	4.5	30.8
27	11.5	10.8	10.5	1.2	29.3	75	9.9	9.2	8.8	1.8	30.8
28	11.3	10.5	10.2	1.4	30.1	76	13.2	12.5	12.2	1.7	30.0
29	14.1	13.4	13.0	1.5	29.6	77	11.6	10.8	10.6	1.7	30.0
30	12.4	11.4	11.2	3.1	30.4	80	12.4	11.7	11.5	1.3	29.8
31	12.5	11.8	11.4	1.0	29.8	81	13.6	12.7	12.3	2.0	29.5
34	11.3	10.6	10.4	0.2	30.2	82	12.1	10.9	10.4	5.4	30.1
35	12.0	11.3	11.0	0.8	29.9	84	11.6	11.0	10.8	0.1	29.2
38	13.4	12.6	12.2	2.0	30.2	87	12.4	11.7	11.3	1.5	29.5
40	12.9	12.3	12.0	0.6	29.5	89	12.2	11.4	11.1	1.6	29.6
43	12.0	11.2	10.8	2.2	30.1	92	13.2	12.3	11.9	2.6	29.6
47	11.1	10.0	10.3	4.3	30.7	93	13.0	12.2	12.0	1.2	29.4
48	12.7	11.7	11.3	3.1	29.6	97	11.3	10.4	10.1	2.5	30.0
49	11.7	11.0	10.7	1.6	30.2	98	11.7	11.0	10.9	0.6	29.9
52	11.7	11.0	10.7	1.5	30.3	99	12.7	11.9	11.6	1.5	29.1
53	12.1	11.3	11.0	1.7	29.8	104	10.2	9.3	8.8	2.9	30.3

4. Results

For the discussion of the results we split the stars in IC348 into three classes: The known proper motion cluster members (which at the same time are the early type stars), the Hα stars, and the X-ray sources which are neither Hα stars nor known cluster members.

For the statistical analysis we used the statistics package ASURV (LaValley et al. 1992). In this package *survival analysis* techniques, necessary for data that include upper limits, are used.

4.1. The early type stars

Here we will denote all stars with spectral type not later than F as early type stars. Only for these stars cluster membership information is available. Since the earliest type star is B5, the X-ray emission of these stars is of special interest, because (with the exception of the late F stars) they should not show intrinsic X-ray emission: They lack the magnetically driven coronae that produce X-ray emission in late type stars as well as strong radiation driven stellar winds with shocks that cause X-ray emission in O and early B stars (see Pallavicini 1989). Indeed, main sequence late B and A stars usually show no or at most

Table 4. Properties of the proper motion cluster members; near infrared data are from Lada & Lada (1995), extinction values from Strom et al. (1974); 90% confidence upper limits for count rates and X-ray luminosities for undetected stars are given.

Object	IC348-X	SpT	J	H	K	A_V	$cr_{\rm PSPC}$	$cr_{\rm HRI}$	log L_X
			[mag]	[mag]	[mag]	[mag]	[cnts/ksec]	[cnts/ksec]	[erg/sec]
G2	14	F9	10.3	9.7	9.5	1.8	23.3 ± 1.3	6.5 ± 0.7	31.4 ± 0.2
G4	–	A0V	8.9	8.8	8.7	1.5	< 0.75	< 0.24	< 29.2
G5	–	A2V	8.9	8.8	8.7	1.4	< 0.75	< 0.24	< 29.2
G6	–	F0	10.1	9.8	9.7	1.5	< 0.50	< 0.17	< 29.0
G8	46	F8	10.6	10.2	10.1	2.8	4.5 ± 0.5	0.6 ± 0.2	30.3 ± 0.1
G9	–	F2	9.3	9.0	8.8	2.3	–	< 0.20	< 29.2
G10	–	A2V	9.8	9.6	9.4	2.7	< 0.45	< 0.57	< 29.3
G11	–	F0	8.5	8.3	7.9	2.2	< 0.81	< 0.27	< 29.4
BD+31°643	–	B5V	7.7	7.6	7.0	2.8	< 1.90	< 0.18	< 29.2
G12	65	A2III	8.3	8.0	7.4	3.2	17.5 ± 1.0	2.0 ± 0.3	30.9 ± 0.1
G13	68	F8	9.2	8.6	8.2	3.8	22.6 ± 1.2	6.8 ± 0.4	31.0 ± 0.1
G16	88	A0	8.5	8.2	7.7	3.7	18.3 ± 1.1	6.8 ± 0.7	31.0 ± 0.1
G17	102	G1III	10.0	9.6	9.4	1.4	3.3 ± 0.5	0.7 ± 0.3	29.9 ± 0.1
F21	–						1.13	–	
F24		B5				2.7	–	< 0.35	< 29.5
F4M	55						1.0 ± 0.6		
F6M	–						–	2.46	

very weak X-ray emission (Schmitt et al. 1993; Cassinelli et al. 1994).

In contrast to this expectation, Zinnecker & Preibisch (1994) detected X-ray emission from 11 out of 21 surveyed Herbig Ae/Be stars. Several possible explanations have been proposed to explain this (see Zinnecker & Preibisch 1994; Caillault et al. 1994; Preibisch & Zinnecker 1995), mostly based on the youth of the Herbig Ae/Be stars or their companions. Thus it is very interesting to look at the X-ray emission of the early type stars in IC348, that are *not* Herbig Ae/Be stars, but certainly young stars.

Five of the 13 early type stars classified as cluster members by Frederick (1956) were detected as X-ray sources; for the undetected stars we determined upper limits to the X-ray luminosity (see Table 4). It is interesting to look at the detection frequency in the spectral classes: While none of the two late B stars is detected, 2 of 5 A stars and 3 of 6 F stars are detected. For the late F stars X-ray emission can be explained by a corona, but not so for the detected A stars G12 and G16. A possible explanation in these cases may be that the X-rays originate not from the A stars themselves, but from close late type companions. We can get some information about this possibility from the NIR colours, since the presence of a late type companion, especially if this companion is a CTTS, should cause an infrared excess. If we compare the *dereddened* $H-K$ colours of the two A stars with the intrinsic colours for their spectral types (Bessell & Brett 1985), we find significant NIR excess for both: $\Delta(H-K) = 0.36$ for G12 and $\Delta(H-K) = 0.25$ for G16. This may indicate the presence of late type companions. It is also worth noting that for both stars the X-ray luminosities as well the the plasma temperatures found in the spectral fits are quite similar to the values found for the late type stars. So the X-ray emission may indeed come from late type companions. Taken together, we find no evidence that stars with spectral types between B5 and F5 in IC348 are intrinsic X-ray emitters.

Let us briefly mention the two brightest stars in IC348, o Per and BD $+31°$ 643:

o Per (X-36) is thought to lie a few parsecs beyond the cluster (Bachiller et al. 1987). Although it is not a cluster member according to Frederick (1956), it may be related to the cluster (see Strom et al. 1974) and also be a young star. It is a spectroscopic binary with a period of 4.4 days (Lynds 1960). The primary is a B1 III star, the secondary is probably a B1V star (Foy 1972). It is worth noting that the IRAS source 03411+3207 is coincident with o Per. The X-ray spectrum we extracted for o Per contains only 165 source counts, so the spectral parameters cannot be evaluated very well. For the fit of the spectrum we fixed $N_{\rm H}$ to the value $1.6 \times 10^{21}\,{\rm cm}^{-2}$ taken from Snow et al. (1994). The X-ray luminosity found by us (see Tab. 2) gives $L_{\rm X}/L_{\rm bol} \approx 5 \times 10^{-9}$, which is rather low but still in the typical range for early B stars (Cassinelli et al. 1994).

BD $+31^\circ\,643$ is a double star[1], with components having a separation of $\lesssim 1''$ and a magnitude difference of 0.2 mag. The secondary is also an early type star, probably a slightly later B star than the primary (Snow et al. 1994). We could not detect X-rays from BD $+31^\circ\,643$. Using the dereddened V magnitude given in Strom et al. (1974) to calculate the bolometric luminosity and our upper limit to the X-ray luminosity as given in Table 4, we found $L_{\rm X}/L_{\rm bol} \leq 2.6 \times 10^{-8}$.

4.2. Late type stars

4.2.1. Hα stars

Although no membership information based on proper motions is available, we assume all Hα stars to be cluster members. From previous studies, 18 Hα stars were known in IC348 (LHα 85 – 100 and LkHα 329 – 330). In January 1990 one of us (G.H.H.) took CCD grism frames of a field with about 6.5 arcmin in diameter with the University of Hawaii 2.23 m (88-inch) telescope on Mauna Kea. The observations were sensitive to the continua of stars of up to $R = 19.5$, and the Hα emission of stars considerably fainter. The dispersion was 440 Å mm^{-1}, or about 6 Å/pixel and the detection threshold for Hα emission in adequately exposed spectra was about 3 Å. These observations conducted at the Institute for Astronomy in Hawaii led to the detection of 31 new Hα stars, which we denote with the prefix "IfAHα". The positions of these stars were determined on direct images obtained at the same telescope in 1993 and 1994. They were reduced to α and δ by reference to a network of 10-12 HST Guide Star Catalog stars on the same frames. The internal agreement (i.e. when the α and δ of the GSC stars were recalculated with the resulting plate constants) averaged about 0.1 arcsec in both coordinates. Nearly all Hα stars could be identified with NIR sources and for most of them (with the exception of a few very faint stars) we could estimate the extinction from the NIR colours as described in Section 3.1.

For a few stars identification was difficult: The stars LkHα 329 and LkHα 330 are located in the field of view of the PSPC observation, but they lie nearly exactly behind the broad ring of the PSPC window support structure and outside of the HRI field of view. So we were not able to investigate their X-ray properties.

The stars IfAHα40 and IfAHα41 form a close pair with a separation of only $\approx 2''$. No HRI source is detected at their positions and the location of the PSPC source X-79 is $\approx 0.5''$ from IfAHα40 and $\approx 3.0''$ from IfAHα41. We assume IfAHα40 to be the X-ray source, although IfAHα41 is also inside the X-ray error circle. It should be noted that the separation between these stars is too small for being resolved in the NIR images of Lada & Lada (1995). There is one NIR source, clearly coincident with IfAHα40, but IfAHα41 may have influenced the measured magnitudes, and the derived extinction may be in error.

The very faint star LHα 94 ($m_{\rm phot} \approx 19.5$) is only $\approx 4''$ away from a much brighter ($V = 15.2$) star, that shows no Hα emission. No NIR source is detected at the position of LHα 94. The position of the X-ray source X-64 in the HRI image is a few arcseconds south of the middle between both stars with approximately equal distance to LHα 94 and the brighter star. In the PSPC image the source is nearly exactly at the position of LHα 94. So we decided to assume LHα 94 to be the X-ray source.

The identification of the X-ray source X-83 with IfAHα45 is questionable due to the large discrepancy of the positions. We keep this identification because the positional error of this weak source is large and IfAHα45 is still the closest optical and NIR counterpart.

For some stars we could not determine a meaningful PSPC upper limit due to the presence of a nearby source.

The individual extinctions estimated from the NIR colours were used to calculate the X-ray luminosities and upper limits given in Table 5. We also calculated Hα-luminosities of the stars for which $W({\rm H}\alpha)$, R, and A_V are available in the following way: We assumed the flux density of a star having $R = 0$ as $2.1 \times 10^{-9}\,{\rm erg/(cm^2 sec Å)}$ (Hayes & Latham 1975; Bessell 1979) and calculated the Hα-luminosities assuming the extinction at Hα to be $0.82 \times A_V$. We cannot find any significant correlation between $L_{{\rm H}_\alpha}$ and $L_{\rm X}$. This is consistent with the results of Bouvier (1990) and indicates that for the CTTS a large fraction of the Hα emission is not of chromospheric origin.

4.2.2. Other X-ray sources in the cluster

No proper motion membership information is available for faint late type (G-M) stars in IC348. However, based on the X-ray properties, we can assume all X-ray sources in the central $20' \times 20'$ to be late type cluster members. We choose the size of this region from the appearance of the cluster on the POSS plate and from the availability of NIR observations that are in most cases the only way to derive extinction estimates. This assumption is based on the following facts:

We can expect that all early type foreground stars have been found in the study of Frederick (1956). Late type foreground stars (with the possible exception of K and M stars) should have an $L_{\rm X}/L_{\rm bol}$ ratio considerably smaller than found for our X-ray sources. Contamination due to background sources is improbable, because the large extinction in the molecular cloud should prevent background stars from shining through the cloud.

So the only contamination to be expected is due to foreground K and M dwarfs. We can estimate this conta-

[1] In the Aitken double star catalog BD $+31^\circ\,643$ appeares as ADS 2730 and is quoted to be even a triple system with G12 as the third component. In consideration of the high density of stars in IC348, we think the rather large separation of $23.5''$ does not justify to assume any relation between G12 and BD $+31^\circ\,643$.

Table 5. Properties of the Hα emission line stars; near infrared data are from Lada & Lada (1995); $L_{\mathrm{H}\alpha}$ gives the Hα luminosity, for some stars only estimates of *w*eak, *m*edium or *s*trong Hα flux are available; 90% confidence upper limits for count rates and X-ray luminosities for undetected stars are given.

Object	IC348 X	W(Hα) [Å]	log $L_{\mathrm{H}\alpha}$ [erg/sec]	R [mag]	J [mag]	H [mag]	K [mag]	$A_{V,\mathrm{IR}}$ [mag]	cr_{PSPC} [cnts/ksec]	cr_{HRI} [cnts/ksec]	log L_X [erg/sec]
IfAHα5	–			18.49	13.6	13.0	12.6		< 0.43	< 0.23	
IfAHα11	–			17.37	12.9	12.1	11.6	2.3	< 0.70	< 0.33	< 29.4
IfAHα12	–			17.37	12.7	12.1	11.7	0.5	< 0.48	< 0.24	< 28.8
IfAHα13	–			18.26	13.0	12.3	11.8	1.4	< 1.71	< 0.55	< 29.5
IfAHα14	–			17.34	11.9	10.6	9.7	5.0	< 2.05	< 0.45	< 30.0
IfAHα15	–	48	29.95	16.69	12.5	11.7	11.4	1.8	< 0.33	< 0.14	< 29.0
IfAHα16	39			16.69	12.5	11.6	11.3	2.7	< 0.9	0.8 ± 0.2	29.9 ± 0.2
IfAHα17	–	33	30.81	16.67	12.3	11.2	10.6	4.9	< 0.35	< 0.22	< 29.6
IfAHα18	–	5	29.25	16.23	12.4	11.6	11.3	2.1	–	< 0.53	< 29.7
IfAHα21	42	54	30.54	16.73	12.2	11.0	10.2	3.5	1.7 ± 0.6	0.5 ± 0.2	30.0 ± 0.2
IfAHα24	50	48	29.91	17.04	12.2	11.2	10.6	2.1	3.6 ± 0.5	< 0.3	30.1 ± 0.2
IfAHα25	–	80	31.09	18.01	12.8	11.5	10.8	6.2	< 0.42	< 0.27	< 29.8
IfAHα26	–			19.53	14.7	14.1	13.6		< 0.96	< 0.19	
IfAHα27	–	38	28.62	18.61	13.4	12.6	12.1	0.4	< 0.46	< 0.27	< 28.8
IfAHα29	–	150			14.9	13.6	12.3	4.5	< 0.24	< 0.31	< 29.3
IfAHα31	–			18.08	13.3	12.3	11.8	1.5	< 0.30	< 0.30	< 28.9
IfAHα32	–			18.45	13.5	12.9	12.5		< 0.58	< 0.35	
IfAHα34	–	32	28.42	18.67	13.1	12.3	11.8	0.1	< 0.97	< 0.19	< 28.8
IfAHα35	–			15.72	11.6	10.5	9.7	2.9	–	< 0.48	< 29.7
IfAHα36	74	11	30.12	15.73	11.9	10.9	10.5	3.1	4.3 ± 0.7	1.0 ± 0.2	30.4 ± 0.2
IfAHα37	–			17.77	13.2	12.4	12.1	2.3	< 0.36	< 0.16	< 29.1
IfAHα40	79	40	30.04	16.83	12.0	10.9	10.2	2.5	0.9 ± 0.4	< 0.2	29.6 ± 0.2
IfAHα41	–	60		17.03							
IfAHα42	–			20.13	15.5	14.6	14.3		< 0.67	< 0.28	
IfAHα45	83	155	29.50	18.03	12.9	12.1	11.6	0.5	1.0 ± 0.5	< 0.2	29.2 ± 0.2
IfAHα46	85	25	29.76	17.20	12.9	11.8	11.1	2.7	< 1.3	1.0 ± 0.1	30.0 ± 0.2
IfAHα47	–			16.95	12.4	11.5	11.1	3.3	< 0.41	< 0.18	< 29.4
IfAHα55	62	3	29.08	16.34	12.0	11.1	10.8	2.4	1.0 ± 0.4	< 0.6	29.6 ± 0.2
IfAHα56	–	4	29.09	16.63	12.2	11.4	11.0	2.4	< 2.62	< 0.63	< 29.8
IfAHα57	69	5	29.53	16.28	12.2	11.3	10.9	3.0	4.5 ± 0.6	1.2 ± 0.2	30.4 ± 0.3
IfAHα58	45	2	28.85	15.82	12.1	11.3	11.0	1.6	1.9 ± 0.4	0.7 ± 0.2	29.7 ± 0.2
LHα85	–	m							< 0.83	< 0.72	
LHα86	9	m			11.9	11.1	10.7	2.1	2.2 ± 0.5	2.2 ± 0.5	30.2 ± 0.2
LHα87	19	s			12.0	11.2	10.7	2.3	1.4 ± 0.4	< 0.5	29.7 ± 0.2
LHα88	18	w		16.09	12.1	11.3	10.7	0.6	2.5 ± 0.5	0.7 ± 0.2	29.6 ± 0.2
LHα89	–	s			13.1	12.1	11.3	2.1	–	< 0.31	< 29.4
LHα90	41	w			12.3	11.5	11.3	1.8	3.1 ± 0.5	1.7 ± 0.2	30.0 ± 0.2
LHα91	44	m			12.4	11.5	11.1	2.2	1.9 ± 0.4	0.7 ± 0.2	29.8 ± 0.2
LHα92	51	21	31.37	13.72	10.1	9.0	7.9	3.6	2.8 ± 0.4	1.1 ± 0.2	30.6 ± 0.2
LHα93	–	106	30.79	15.70	11.8	10.8	10.2	2.1	< 0.47	< 0.26	< 29.2
LHα94	64	4							6.4 ± 0.6	1.4 ± 0.2	
LHα95	–	53			11.6	10.5	9.7	2.9	–	< 0.60	< 29.9
LHα96	–	w							< 0.55	< 0.71	
LHα97	86	s			10.9	9.9	9.3	2.0	1.9 ± 0.5	1.4 ± 0.5	29.8 ± 0.2
LHα98	94	w			10.9	10.0	9.5	3.1	5.9 ± 0.8	3.8 ± 0.3	30.6 ± 0.2
LHα99	–								< 0.48	< 0.51	
LkHα100	–	w							< 0.36	< 0.52	

mination from the outer parts of the PSPC image: There we find only 9 X-ray sources in the region more than 25′ from the center. If this is typical for the surface density of foreground X-ray sources, we can calculate the expected number of foreground sources inside the central $20' \times 20'$. Assuming the sensitivity in the central region to be on average 2.5 times higher than in the outer ring, we expect 1–2 contaminating sources. The number of expected foreground sources can also be estimated using the X-ray luminosity function of the K and M stars in the solar neighborhood as given in Schmitt et al. (1995). With a method developed by Schmitt & Snowden (1990) the following formula for the number N of expected foreground sources can be derived:

$$N = 2.9 \times 10^4 \ \Omega \ \left(\frac{S_{\rm min}}{10^{-14}\,{\rm erg/(sec\,cm^2)}} \right)^{-3/2}$$

Here Ω is the solid angle of the region of interest, $S_{\rm min}$ is the minimal detectable X-ray source flux and a mean density of 0.065 $\rm pc^{-3}$ for the K and M stars is used (see also Randich et al. 1995). From the count rates of the weakest sources we estimate $S_{\rm min} \approx 8 \times 10^{-15}\,{\rm erg/(sec\,cm^2)}$. Thus, for the central $20' \times 20'$ region we get $N = 1.4$, in perfect agreement with the estimate above. So with only one or two exceptions all of the 56 X-ray sources are most probably members of IC348.

4.3. X-ray luminosity and bolometric luminosity

For the cluster members investigated by Strom et al. (1974) we calculated the bolometric luminosity from the dereddened magnitude. For the late type stars, where no spectral type and optical colour is available, we use a method developed by Greene et al. (1994): For young stars in several star-forming regions they found a good correlation between the bolometric luminosity and the dereddened J band flux J_0. This correlation could be confirmed with theoretical models of pre-main sequence stars. From their correlation we can derive the following formula for the bolometric luminosities in IC348:

$$\frac{L_{\rm bol}}{L_\odot} = (18\,550 \pm 900)\,10^{-J_0/2.5} - (0.06 \pm 0.11)$$

These luminosity estimates can be used to look for a proportionality between $L_{\rm X}$ and $L_{\rm bol}$ for the late type cluster stars as found for several other star forming regions. Excluding the early type stars and stars with $\log L_{\rm bol}/L_\odot \geq 0.5$ and using the ASURV software package to take into account the upper limits we find the correlation:

$$\log L_{\rm X}[{\rm erg/sec}] = (30.1 \pm 0.2) + (0.9 \pm 0.3)\log(L_{\rm bol}/L_\odot)$$

This is very similar to the correlations found for the late type stars in the Chameleon I cloud (slope 1.1 ± 0.2; Feigelson et al. 1993) and in the ρ Ophiuchi cloud core (slope 1.1 ± 0.2; Casanova et al. 1995)

In Fig. 4 we show the relation between X-ray and bolometric luminosity for all stars. For the low luminosity stars with $\log(L_{\rm bol}/L_\odot) < 0.5$ we find $\log(L_{\rm X}/L_{\rm bol})$ between -4 and -2, while for most of the more luminous early type stars this ratio is much lower. A very similar behaviour was found for the stars in the Orion nebula by Gagné & Caillault (1994). These results are a further justification for the assumption of all unclassified X-ray sources being cluster members, since late type field stars and giants usually show $\log(L_{\rm X}/L_{\rm bol}) \lesssim -6$ (Pallavicini 1989).

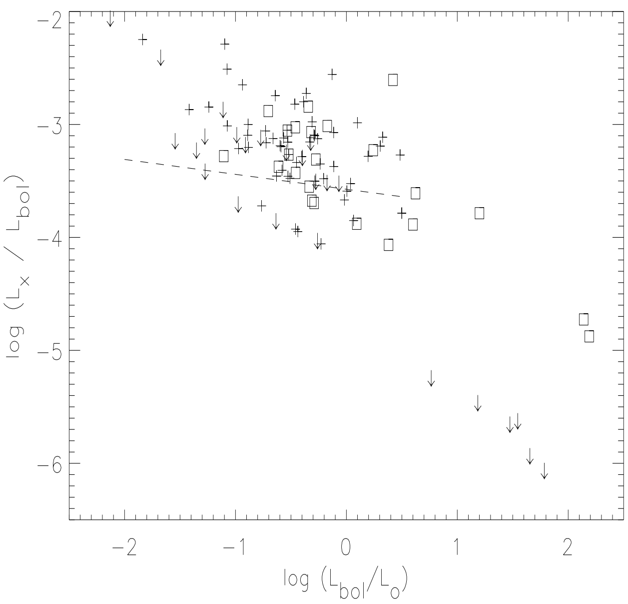

Fig. 4. Relation between X-ray and bolometric luminosity: Stars with unknown cluster membership are drawn as crosses, known cluster members and Hα stars are drawn as squares or downward arrows for upper limits. The dashed line shows the empirical relation found with ASURV for the low mass stars.

Even more evidence for this can be found in the NIR colour-colour diagram (Fig. 5). With only one exception, all unclassified X-ray sources show NIR colours consistent with those of reddened main-sequence stars. This means that they are most probably WTTS.

To investigate the collective properties of the X-ray sources, we calculated the maximum-likelihood Kaplan-Meier estimator of the cumulative luminosity distribution function. It is very similar to those of other young clusters (see Fig. 6 of Gagné et al. (1995) for a comparison). The median of the X-ray luminosity is $\log L_{\rm X} \approx 30.0$, the integrated X-ray luminosity is $\approx 1.6 \times 10^{32}$ erg/sec.

4.4. X-ray properties of the T Tauri stars

A very interesting question is whether CTTS and WTTS have systematically different X-ray luminosities. Quite

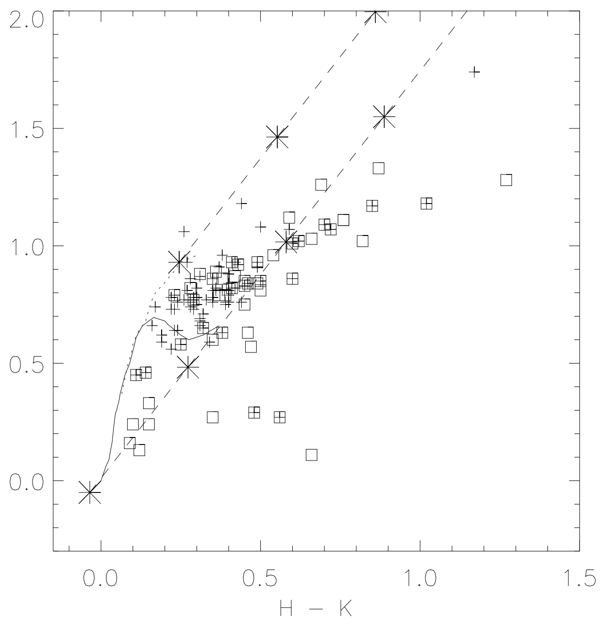

Fig. 5. NIR colour-colour diagram of the X-ray sources (crosses) and the known cluster members and Hα stars (squares) based on the NIR colours of Lada & Lada (1995). The solid line shows the colours for main sequence stars, the dotted line for giants. The dashed lines show the reddening path on which asterisks have been placed at intervals of $A_V = 5$ mag.

confusing results have been reported in different studies: In the Taurus-Auriga molecular cloud (Neuhäuser et al. 1995) and in the Lupus star forming region (Wichmann 1994) the WTTS seem to be considerably stonger X-ray emitters (by factors between 4 and 10) than the CTTS. For the Orion nebula region (Gagné et al. 1995) and the Chameleon I cloud (Feigelson et al. 1993) only small and merely significant differences have been found. Finally, Casanova et al. (1995) could not find any systematic differences for the X-ray luminosities of the CTTS and WTTS in the ρ Ophiuchi cloud core.

Systematically higher X-ray luminosities of the WTTS compared to the CTTS could be explained in the model of magnetospheric accretion (Camenzind 1990; Königl 1991), where extended magnetic fields from the surface of the TTS couple to the accretion disk. This connection could prevent stars with massive disks from spinning up and regulate the rotation of the TTS (see Edwards et al. 1993). Since the X-ray activity of the TTS seems to be related to the stellar rotation, this model predicts a lower X-ray luminosity for CTTS with their more massive disks compared to the WTTS.

To investigate this question with our data we performed several tests. First, we concentrated on the Hα stars and split them into the group of classical T Tauri stars (CTTS) with $W(\mathrm{H}\alpha) \geq 10$ Å or strong Hα flux and the group of weak line T Tauri stars (WTTS) with $W(\mathrm{H}\alpha) < 10$ Å or weak Hα flux. Stars for which the strength of the Hα emission line was too small to determine $W(\mathrm{H}\alpha)$ were assumed to be WTTS. Of the 18 CTTS investigated, 9 were detected as X-ray sources, giving a detection frequency of $(50 \pm 12)\%$. For the WTTS the detection frequency is 7 out of 17 $((41 \pm 12)\%)$. This implies no significant difference in the detection frequencies. Comparing the X-ray luminosities of the CTTS and the Hα selected WTTS we could not find any indication of systematic differences: The two-sample test in ASURV gave probabilities between 0.7 and 0.8 that the distributions of X-ray luminosities are equal for both samples. As described in the previous section, we could not find any significant correlation between the Hα luminosity and the X-ray luminosity.

For a second series of tests we used a more complete sample of WTTS by including the 56 X-ray sources without Hα emission. If we compare this sample of Hα- *and* X-ray selected WTTS to the CTTS, we find significant differences in the X-ray luminosity functions: The Kaplan-Meier estimates of the X-ray luminosity functions are different with a confidence of at least 96% and give a 4 times higher median for the WTTS compared to the CTTS. This is in very good agreement with the results of Neuhäuser et al. (1995) for the TTS in the Taurus-Auriga region.

It must be emphasized, however, that there is a serious selection effect due to the definition of our samples: From the deep Hα observations we can assume to know the complete sample of the CTTS. On the other hand, as far as the WTTS are concerned, we only know those objects that either show Hα emission with $W(\mathrm{H}\alpha) \geq 3$ Å or are detected as X-ray sources. So we miss the WTTS with very weak Hα emission ($W(\mathrm{H}\alpha) < 3$ Å) and not detectable X-ray emission. These objects may represent a considerable fraction of the WTTS: About 60% of the known WTTS with Hα emission were not detected as X-ray sources. If the X-ray detection frequency is independent of Hα emission, we must assume that a considerable fraction of the WTTS not detected as Hα stars were also not detected as X-ray sources and thus are missing in our WTTS sample. Since these missing objects are weak X-ray sources, the sample of the Hα- *and* X-ray selected WTTS might considerably overestimate the mean X-ray luminosities of the WTTS.

On the other hand, this is not a specific problem for our study in IC348, since the vast majority of all known pre-main-sequence stars were detected either due to their Hα- or their X-ray emission. Pre-main-sequence stars lacking both indicators are very hard to find.

4.5. Influence of the X-rays on the molecular cloud

The high spatial density of X-ray sources makes it worthwhile to investigate the possibility of a feedback of the X-radiation on the parental molecular cloud. Such a feedback could occur due to an enhancement of the fractional ionization of the cloud caused by the X-rays (Silk & Norman 1983). Through processes like ambipolar diffusion the ionization fraction can have crucial influence on the early stages of star formation (e.g. Shu et al. 1987).

Casanova et al. (1995) have addressed this question for the ρ Ophiuchi star forming region. Based on the results of Krolik & Kallman (1983) they give an improved formula for the estimation of the minimum ionization rate caused by the X-ray sources. From our ROSAT image we estimate that at least half of the total X-ray luminosity is emitted by the ≈ 80 sources in the central $10'$ ($\widehat{=}\, 0.87\,\mathrm{pc}$). Hence we assume an average source separation of 0.2 pc and a total X-ray luminosity of $\approx 10^{32}$ erg/sec for the central region. Using further a source temperature of $kT \approx 1$ keV and an extinction of $A_{V,\max} \approx 7.5$ mag we obtain a minimum ionization rate of $\zeta_{\mathrm{X}} \approx 2 \times 10^{-17}\,\mathrm{s}^{-1}$. This has to be compared to the ionization rate caused by galactic cosmic rays, which usually is assumed to be around $10^{-18} - 10^{-17}\,\mathrm{s}^{-1}$, although values up to $\lesssim 10^{-16}\,\mathrm{s}^{-1}$ have been determined for some molecular clouds (Black et al. 1990). Thus the ionization of the molecular cloud in IC348 may indeed be dominated by the X-ray emission from the young stars. Since a considerable enhancement of the ionization fraction can probably hinder further star formation (Silk 1985, Ciolek & Mouschovias 1994), the dense cluster of X-ray sources may influence the further evolution of the cluster.

5. X-ray Variability

Young stars often show strong X-ray variability. In their EINSTEIN study of the ρ Oph dark cloud Montmerle et al. (1983) found that most X-ray sources were variable with factors up to 10 on time scales of a few days. Strong variability has also been reported for other young clusters (e.g. Gagné & Caillault 1994).

Our data are very well suited to search for variability: We can examine the X-ray lightcurves for short-term variability and we can compare the count rates in the PSPC and HRI and ROSAT All-Sky Survey observations to look for long-term variability.

5.1. Short-term variability

To investigate the short time variability, we applied a Kolmogorov-Smirnov test to the lightcurves of all sources. This tests the hypothesis that the source is constant and gives the probability that the source is variable. We found that 46 sources are variable with more than 99.7% probability. We investigated the lightcurves of these sources in detail and found eight strong X-ray flares: The strongest is the flare on LHα 92, for which the count rate rises by more than a factor of 300 (a detailed analysis of this event is given in Preibisch et al. 1993; please note that there the star is erroneously denoted as LkHα 92). For every flare we tried to determine the rise and exponential decay times, the amplitudes defined as the ratio of the maximum and the pre-flare count rate, and the total X-ray flare energy. These properties are given in Table 6. For some of the flares we could not determine all properties, e.g. if the flares occurred very close to the end of the observation.

It is worth taking note of the large energy output of these flares: While even the largest flares on the Sun usually do not exceed $\approx 10^{31}$ erg, the energy of these flares is 3 to 5 orders of magnitude higher. Such large flare energies seem to be typical for very young stars: In a systematic study of ROSAT observations of star forming regions and young clusters Preibisch & Neuhäuser (1995) found 36 large flares on young stars. The most energetic flares, just in the range of the flares found in IC348, were found on the youngest stars.

Table 6. Properties of X-ray flares: count rate amplitude, decay time τ, rise time t_r and total X-ray flare energy E_{X}.

IC348-X	amplitude cr_f/cr_0	τ [hours]	t_r [hours]	log E_{X} [erg]
4	9	1.9	1.0	–
20	14	0.6	1.4	34.2
30	8	–	–	–
51	300	2.2	0.5	36.6
63	3	2.2	1.0	34.4
73	3	1.9	1.0	34.7
85	21	–	–	–
86	18	–	–	–

5.2. Long-term variability

To evaluate variability on time scales of several years, we compared the PSPC and HRI count rates of the 49 common sources. The sensitivity of the HRI is smaller than that of the PSPC. We have calculated the sensitivity ratio assuming optical thin plasma emission (Raymond & Smith model) with $T = 10^7$ K for different values for the X-ray extinction. Raising the extinction from $N_{\mathrm{H}} = 6.5 \times 10^{19}\,\mathrm{cm}^{-2}$ towards $10^{22}\,\mathrm{cm}^{-2}$ causes the ratio to decrease from 2.5 to 2.0. There are nine sources, where the 3σ error region of the countrate ratio is outside the interval [2.0,2.5]. These sources can be regarded to be variable with high confidence. It should be noted that for the sources showing a flare we used the pre-flare count rates to calculate this ratio.

To get further information about long time variability, we also used the results of the ROSAT All-Sky Survey, which was performed in the second half of 1990. When comparing the data of the pointed observations to the

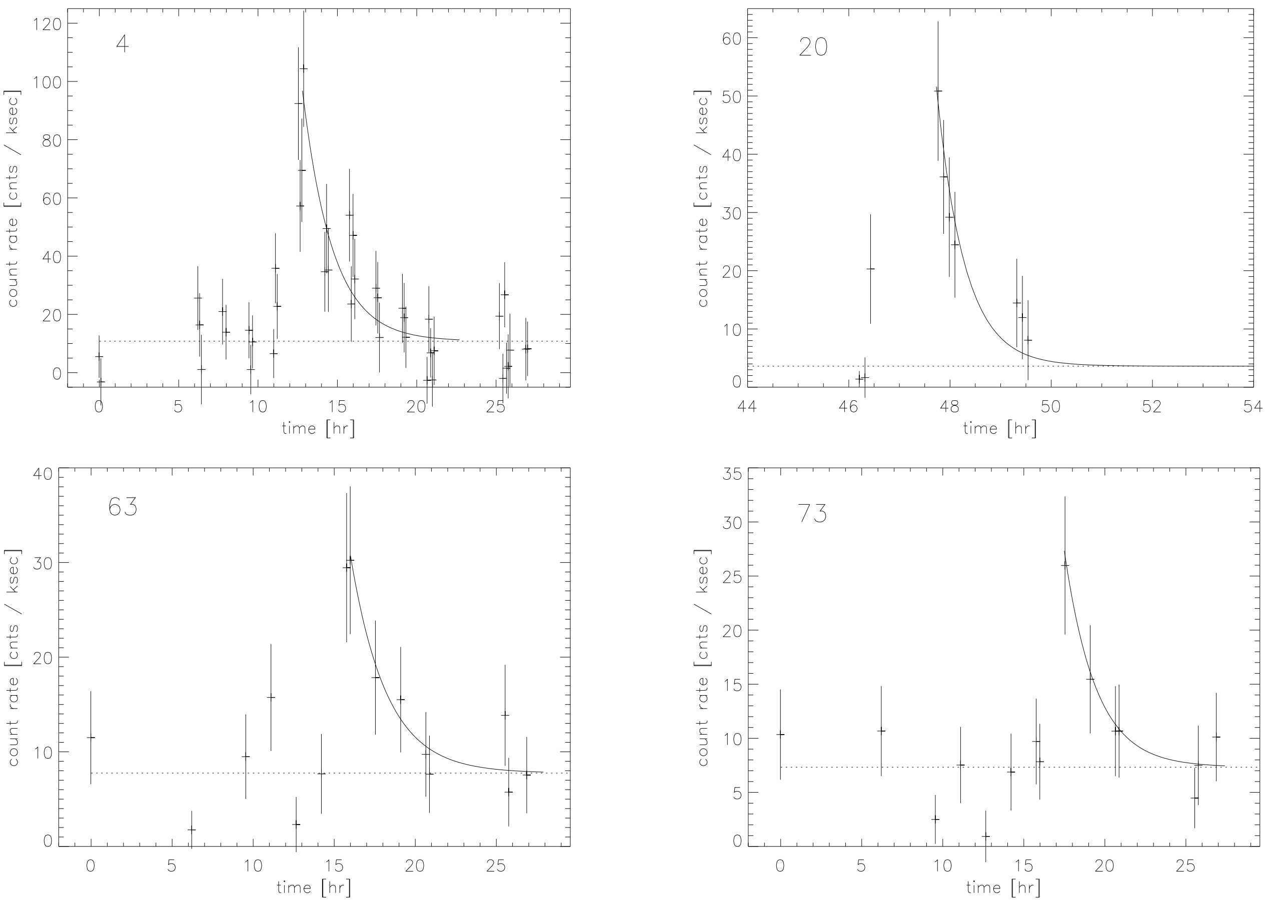

Fig. 6. Lightcurves of some X-ray flares (source number in upper left corner); the solid lines show the fitted exponential decay curves, the dotted lines the medium pre-flare count rates determined from the other time intervals (not shown).

survey data one has to keep in mind the large sensitivity difference. While the exposure time in the survey was only ≈ 400 sec, our pointed observations were about a factor of 60 deeper. This explains, why only five X-ray sources were detected during the survey within the field of view of the PSPC pointing. Two of the survey sources lie in the central cluster of X-ray sources. Due to the low spatial resolution ($\approx 45''$) of the survey data, they probably are the unresolved sum of several sources and cannot be used for further analysis. One survey source corresponds to our source X-114, identified with F23. In our PSPC pointing, this source is located very close to the ring structure of the PSPC entrance window. A partial occultation of this source by this structure can explain why our PSPC count rate is (10.4 ± 1.7) counts/ksec whereas the survey count rate is (18.6 ± 7.9) counts/ksec.

Another survey source corresponds to our source X-88, that is identified with the star GSC 2359 630. Here we find a good agreement between the survey count rate (19.4 ± 7.8 counts/ksec) and the count rate in our PSPC pointing (18.3 ± 1.1 counts/ksec). Together with a PSPC/HRI count rate ratio of 2.7 ± 0.4 these data agree very well.

One survey source has a rather uncertain identification (positional error $33''$) with our source X-6. The survey count rate of (12.7 ± 6.3) counts/ksec is much higher than our PSPC count rate of (2.5 ± 1.0) counts/ksec. Since any shadowing effects can be excluded at the source position, there is evidence for variability. Since the 90% upper limit of 0.6 counts/ksec for the HRI count rate is consistent with the PSPC count rate, the source has perhaps shown a flare during the survey observations.

In total, we could investigate the long term variability of 50 sources. Among these, 9 sources $[(18 \pm 5)\%]$ showed evidence for variability. It has to be emphasized that in our observations we cannot really discern between variability on long or short timescales. A source showing variability within a few days may appear constant during each pointed observation; comparing two pointed observations, it depends on the moment of the observations whether the source appears constant or variable.

5.3. Total X-ray variability

Taken together, 52 sources [$(45 \pm 5)\%$] show variability on short or long timescales. This fraction of variable sources lies between the 80% reported for the ρ Oph sources (Montmerle et al. 1983) and 25% for the Orion cluster members (Gagné & Caillault 1994) and thus seems to be typical for young stars.

6. Summary

We present the first X-ray observations of the young cluster IC348. In a region that has not drawn much attention until recently, we have detected a dense cluster of more than 100 X-ray sources. We show that due to the large total integrated X-ray luminosity of at least 1.6×10^{32} erg/sec the X-ray sources can considerably enhance the ionization fraction of the molecular cloud and influence the further evolution of the cluster.

In many respects the properties of the X-ray sources are quite similar to those of other young stars: The range of X-ray luminosities, L_X/L_{bol}, and the number of X-ray flares are about the same as reported for other young clusters. The early type (B-A) cluster members probably are not intrinsic X-ray emitters. Either they are undetected in our ROSAT images or they display hints of having late type companions.

The WTTS seem to be systematically more X-ray luminous than the CTTS, but this may be at least partially caused by selection effects.

A big problem is that for most stars up to now only little if any optical information is available, and there is a clear need for further observations of this cluster. We have already performed some observations and are currently working on photometry and spectroscopy. Further observations are scheduled in the near future.

Acknowledgements. We are grateful to E. Lada, who provided us with the data of her NIR survey of IC348. Without this data some parts of this work would have been impossible. I. Thiering kindly donated us part of her telescope time to take V- and I-band images of IC348 and R. Neuhäuser kindly provided us with the ROSAT survey data of IC348. D.N. Burrows provided us with the program of R.P. Kraft for calculating Bayesian confidence intervals for the count rates. We acknowledge the use of the Astrophysics Data System (ADS) provided by NASA and the SIMBAD database operated at CDS. We would like to thank the referee for several helpful comments.

This work was supported by the DARA under grant 05 OR 9103 0. The ROSAT project was supported by the Bundesministerium für Forschung und Technologie (BMFT/DARA) and the Max-Planck-Society.

References

Bachiller, R., Cernicharo, J., Goldsmith, P., & Omont, A., 1987, A&A 185, 297
Bessel, M.S., 1979, PASP 91, 589
Bessell, M.S. & Brett, J.M., 1985, PASP 100, 1134
Black, J.H., Van Dishoek, E.F., Willner, S.P., & Woods, R.C., 1990, ApJ 358, 459
Blaauw, A., 1952, Bull. Astron. Inst. Netherlands 11, 405
Bouvier, J., 1990, AJ 99, 946
Caillault, J.-P., Gagné, M., & Stauffer, J.R., 1994, ApJ 342, 386
Camenzind, M., 1990, in: *Reviews in Modern Astrononmy 3*, ed. G. Klare, p. 234
Casanova, S., Montmerle, T., Feigelson, E.D., & André, P., 1995, ApJ 439, 752
Cassinelli, J.P., Cohen, D.H., MacFarlane, J.J., Sanders, W.T., & Welsh, B.J., 1994, ApJ 421, 705
Cernicharo, J., Bachiller, R., & Duvert, G., 1985, A&A 149, 273
Ciolek, G.E., & Mouschovias, T.C., 1994, ApJ 425, 142
David, L.P., Harnden, F.R., Kearns, K.E., & Zombeck, M.V., 1993, *The ROSAT High Resolution Imager*, U.S. ROSAT Science Data Center/SAO
Edwards, S., Strom, S.E., Hartigan, P., et al., 1993, AJ 106, 372
Feigelson, E.D., Casanova, S., Montmerle, T., & Guibert, J., 1993, ApJ 416, 623
Foy, R., 1972, A&A 16, 108
Frederick, L.W., 1956, AJ 61, 437
Gagné, M., & Caillault, J.-P., 1994, ApJ 437, 361
Gagné, M., Caillault, J.-P., & Stauffer, J.R., 1995, ApJ 445, 280
Gingrich, C.H., 1922, ApJ 56, 139
Greene, T.P., Wilking, B.A., André, P., Young, E.T., & Lada, C.J., 1994, ApJ 434, 614
Harris, D.L., Morgan, W.W., & Roman, N.G., 1954, ApJ 119, 622
Hayes, D.S. & Latham, D.W., 1975, ApJ 197, 593
Herbig, G.H., 1954, PASP 66, 19
Königl, A., 1991, ApJ 370, L39
Kraft, R.P., Burrows, D.N., & Nousek, J.A., 1991, ApJ 374, 344
Krolik, J.H., & Kallman, T.R., 1983, ApJ 267, 610
Kunkel, M., 1995, PhD thesis, University Würzburg, in prep.
Lada, E.,A., & Lada, C.J., 1995, AJ 109, 1682
Lampton, M., Margon, B., & Bowyer, S., 1976, ApJ 208, 177
LaValley, M., Isobe, T., & Feigelson, E.D., 1992, BAAS 24, 839
Lasker, B.M., Sturch, C.R., McLean, B.J., et al., 1990, AJ 99, 2019
Lynds, C.R., 1960, ApJ 131, 122
Maggio, A., Sciortino, S., Collura, A., Harnden, F., 1995, A&AS 110, 573
McCaughrean, M.J., Rayner, J.T., & Zinnecker, H., 1994, ApJ 436, L189
Montmerle, T., Koch-Miramond, L., Falgarone, E., & Grindlay, J.E., 1983, ApJ 269, 182
Morrison, R. & McCammon, D., 1983, ApJ 270, 119
Neuhäuser, R., Sterzik, M.F., Schmitt, J.H.M.M., Wichmann, R., & Krautter, J., 1995, A&A 297, 391
Pallavicini, R., 1989, A&A Rev. 1, 177
Paresce, F., 1984, AJ 89, 1022
Predehl, P. & Schmitt, J.H.M.M., 1995, A&A 293, 889
Preibisch, Th. & Neuhäuser, R., 1995, in: *IAU Colloquium 151: Flares and Flashes*, eds. J. Greiner & H. Duerbeck, in press
Preibisch, Th., Zinnecker, H., & Schmitt, J.H.M.M., 1993, A&A 279, L33

Preibisch, Th. & Zinnecker, H., 1995, in: *Röntgenstrahlung from the Universe*, Conference Proceedings, MPE Report
Press, W.H., Flannery, B.P., Teukolsky, S.A. & Vetterling, W.T., 1986, *Numerical recipies*, Cambridge
Randich, S., Schmitt, J.H.M.M., Prosser, C.F. & Stauffer, J.R., 1995, A&A 300, 134
Raymond, J.C. & Smith, B.W., 1977, ApJS 35, 419
Rieke, G.H. & Lebofsky, M.J., 1985, ApJ 288, 618
Savage, B.D., Drake, J.F., Budich, W., & Bohlin, R.C., 1977, ApJ 216, 291
Schmidt-Kaler, 1982, in: Landolt-Bornstein, ed. K.H. Hellwege, Springer Verlag, Berlin
Schmitt, J.H.M.M. & Snowden, S.L., 1990, ApJ 361, 207
Schmitt, J.H.M.M., Collura, A., Sciortino, S., Vaiana, G.S., Harnden, F.R., & Rosner, R., 1990, ApJ, 365, 704
Schmitt, J.H.M.M., Zinnecker, H., Cruddace, R., & Harnden, F.R., 1993, ApJ 402, L13
Schmitt, J.H.M.M., Fleming, T.A. & Giampapa, M.S., 1995, ApJ 450, 392
Shu, F.H., Adams, F.C., & Linzano, S., 1987, ARA&A 25, 53
Silk, J., 1985, in: *Birth & Infancy of Stars*, eds. R. Lucas & A. Omont, p. 349
Silk, J., & Norman, C., 1983, ApJ 272, L49
Snow, T.P., Hanson, M.M., Seab, C.G., & Saken, J.M., 1994, ApJ 420, 632
Strom, S.E., Strom, K.M., & Carrasco, L., 1974, PASP 86, 798
Strom, K.M., Strom, S.E., & Merrill, K.M., 1994, ApJ 412, 233
Trümper, J. et al., 1991, Nature 349, 579
Wichmann, R., 1994, PhD thesis, University Heidelberg
Zimmermann, H.U., Belloni, T., Izzo, C., Kahabka, P., Schwentker, O., 1993, *EXSAS User's Guide*, MPE Report 244, Garching
Zinnecker, H. & Preibisch, Th., 1994, A&A 292, 152

This article was processed by the author using Springer-Verlag LaTeX A&A style file *L-AA* version 3.